Proceedings of the 7th International Symposium on Cavitation
CAV2009 – Paper No. 182
August 17-22, 2009, Ann Arbor, Michigan, USA

Experimental Investigations on the Flow Structure and Turbulence of the Propeller Tip Vortex at Different Cavitation States

Yi-Chih Chow
National Taiwan Ocean University
Keelung, Taiwan (R.O.C.)

Wen-Chuan Tsai
National Taiwan Ocean University
Keelung, Taiwan (R.O.C.)

Yaw-Huei Lee
National Taiwan Ocean University
Keelung, Taiwan (R.O.C.)

ABSTRACT

In a previous series of open water tests for a certain marine propeller, we kept decreasing the advance coefficient and observed the propeller tip vortex going through a process from non-cavitating to cavitating and back to non-cavitating but micro-bubble-filled conditions. This process provides an excellent opportunity for investigating the flow structure and the turbulence associated with the tip vortex under different statuses of cavitation. Particle image velocimetry technique is used to measure the instantaneous velocity distributions at six experimental conditions parameterized with the advance coefficient and the cavitation number. The results show that the mean circulation (or mean kinetic energy) of either the cavitating or the micro-bubble-filled tip vortex is greater than that of the single-phase (liquid) counterpart, whereas the turbulent kinetic energy associated with the tip vortex has an opposite trend. These phenomena imply that extraordinary kinetic energy sources/transfers within the flow exist due to interactions between the vapor and the liquid phases of the tip vortex fluid.

INTRODUCTION

Our previous work (Chow et al. [1]) attempted to clarify the origin of the formation of "fog-like micro-bubble cluster" (FMBC) observed with a typical six-blade, NACA-profile propeller operating in a uniform flow. Figure 1 shows the dramatic change from a clear propeller tip vortex cavity (Fig. 1a, at a higher advance coefficient) to a FMBC (Fig. 1b, at a lower advance coefficient). This phenomenon was at first speculated as a result of the tip vortex cavitation (TVC) bursting (see English [2]). However, by combining experimental (including flow visualization and particle image velocimetry, PIV), numerical, and theoretical approaches, Chow et al. [1] reached a quite different conclusion that the sheet cavitation, i.e., the attached cavitation on the suction side of the propeller, causes reduction of the pressure drop from the outside to the inside of the tip vortex and thus suppresses the TVC, and simultaneously generates the FMBC that later gets entrained into the tip vortex. This finding may have a significant impact on the concept of propeller design, which at the present stage doesn't take into consideration the effect of sheet cavitation on the TVC.

While the aforementioned work focuses on the mechanism of the FMBC phenomenon, the present study continues that effort but directs the attention to the flow structure and the turbulence of the tip vortex, which undergoes the vanishing process of TVC described in [1]. As a matter of fact, the flow in the wake of a propeller is complicated and turbulent (e.g., Lee et al. [3] and Calcagno et al. [4]). The major complexity of this flow is caused by the tip vortices and associated cavitations. For example, detailed measurements for a ducted rotor done by Chesnakas and Jessup [5] and Oweis and Ceccio [6] have shown interesting phenomena such as the vortex-vortex interactions and their effects. Therefore, it is crucial to accurately model and predict the characteristics of the tip vortex and TVC for propeller design purposes. Kim and Rhee [7] and Rhee and Joshi [8] pointed out that turbulence modeling is one of the two major issues in numerical simulations of the tip vortex flow (the other one is mesh generation). An example that numerically studied the turbulence and its modeling associated with tip vortex flows is Chen [9], who concluded that the Reynolds stresses in the tip vortex flows are difficult to predict using several popular turbulence models.

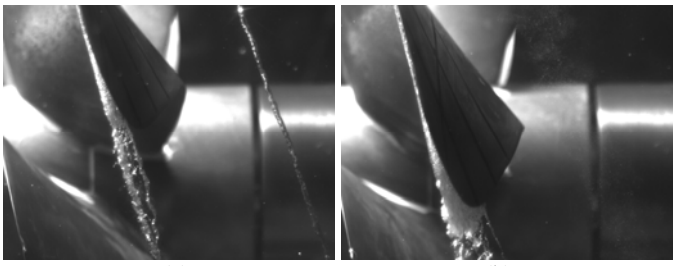

(a) (b)

Figure 1: (a) Tip vortex cavitation, and (b) fog-like micro-bubble cluster.

In the present study, we perform PIV measurements of the tip vortex flow under different experimental conditions that will be explained in the next section: experimental setup. Then results, related analyses, and conclusions follow.

EXPERIMENTAL SETUP

As shown in Fig. 2, we perform PIV measurements of the propeller tip vortex in a cavitation tunnel. This cavitation tunnel is a close-loop, circulation type of water tunnel with pressure control capable of performing de-aeration processes. The cross-sectional area of the test section is 0.5 m × 0.5 m. The maximum flow speed in this facility is 11.7 m/s, and the inflow uniformity can be maintained quite well with several flow straighteners along the loop. An adjustable inclined-shaft dynamometer is integrated with this tunnel. In the present experiment, we only use the dynamometer as the propeller shaft leveled horizontally with rotational speed control.

The PIV system we utilize consists of a 180 mJ/pulse double-head Nd:YAG laser, light-sheet generation optics, a cross-correlation, 15Hz, 1600x1200 pixels, CCD camera (LaVision Image ProX), an image acquisition system capable of synchronization based on the trigger signal from the motor encoder, and hollow glass spheres with an average diameter of 5μm as seeding particles. The light sheet position and the phase angle of the propeller are carefully adjusted for imaging the transverse section of the tip vortex. One thousand image pairs are acquired at a fixed phase for each experimental condition (details follow). PIV images obtained are analyzed using LaVision's DaVis software to generate flow velocity vector maps.

To evaluate the accuracy the analysis algorithms and procedures are able to achieve, we take several images acquired in the measurements and transform them by translation and rotation of known values (in pixel) to form semi-artificial PIV image pairs. Then we feed these manufactured image pairs to the analysis software and compare the outcomes with the known vector maps. The average difference between these two sets of values is found to be 0.6 pixel, which translates to 3% uncertainty in instantaneous velocity with the typical particle image displacement of 20 pixels. Other uncertainty contributors include rotational speed variation, inflow variation and optical misalignment, which are estimated to be almost one order of magnitude less than that incurred in the analysis algorithms and procedures as mentioned above, i.e., they are negligible.

In Chow et al. [1] we used three model propellers: the first one has 5 New-Section blades whose purpose is to reduce the sheet cavitation; the second one has endplates on its five blade tips to suppress its tip vortices; the third one, also the one used in this study, is a six-blade, NACA-profile propeller that generates the FMBC phenomenon. As mentioned in the introduction section, we use this propeller to investigate the flow structure and the turbulence of the tip vortex associated with different statuses of TVC. The two experimental parameters that control the status of TVC are the advance coefficient, *J*, and the cavitation number, σ. Their definitions are:

$$J = \frac{U_0}{nD} \tag{1}$$

and

$$\sigma = \frac{P_r - P_v}{\frac{1}{2}\rho U_0^2} \tag{2}$$

where $U_0 = 5$ m/s is the inflow velocity to the propeller, $n = 22.2 \sim 26.3$ round/s is the propeller rotational speed, $D = 0.25$ m is the diameter of the propeller, P_r denotes the reference pressure of the tunnel, P_v denotes the vapor pressure of the liquid fluid (water), and ρ denotes the density of water. We focus on $J = 0.90$, 0.78 and 0.76, and $\sigma = \sigma_{atm}$ (P_r = atmospheric pressure) and $\sigma_{2.5}$ ($\sigma = 2.5$, and lower than σ_{atm}). TVC statuses under combinations of *J*'s and σ 's are listed in Table 1.

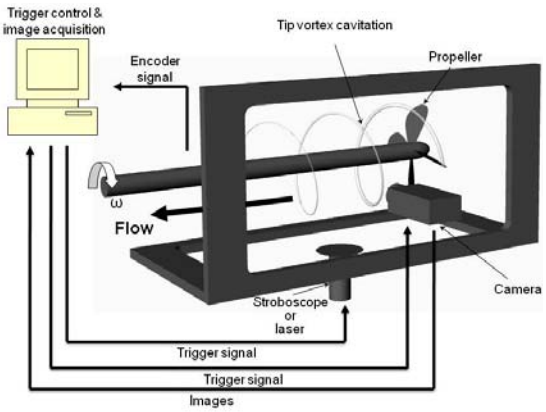

Figure 2: Schematic of the integrated experimental setup.

Table 1: TVC statuses under 6 experimental conditions.

$\sigma \setminus J$	$J = 0.90$	$J = 0.78$	$J = 0.76$
$\sigma = \sigma_{atm}$	No TVC	No TVC	No TVC
$\sigma = \sigma_{2.5}$	No TVC	TVC	FMBC

RESULTS AND DISCUSSION

1. Mean Flow Characteristics:

Each mean flow velocity field is obtained by averaging 1000 realizations at the same phase. Assuming the errors associated with the instantaneous velocities are random, the errors associated with the mean velocities can be estimated as $3\%/\sqrt{1000} \approx 0.1\%$, i.e., it is very small and can be neglected. This phase-averaging procedure also enables us to calculate the Reynolds stresses and related parameters of turbulence (details follow). Figure 3 shows the induced velocity vector maps of tip vortex flows under 6 experimental conditions described by Table 1. They are obtained by subtracting the mean velocity vector at the location where the mean vorticity peaks from the measured velocity vectors. Mean-flow velocity distributions of both cases of $J = 0.90$ being almost identical regardless of σ (i.e., ambient pressure)

difference is expected since no TVC occurs for either case. At ($J = 0.78$, $\sigma = \sigma_{2.5}$) TVC occurs, resulting in strong reflection of laser light during the experiment that overwhelms particle images close to the TVC area and hence no reliable data obtained in that area (Fig. 3d). It is clearly evident that the common characteristics of these mean flow structures are the non-uniformities caused by the propeller wake.

In order to elucidate the major trends of the flow and turbulence, we circumferentially average all the variables as:

$$F(r) = \frac{1}{2\pi}\int_0^{2\pi} f(r,\theta)d\theta \tag{3}$$

where $f(r,\theta)$ is a mean variable and function of polar coordinates (r,θ) whose origin is located at the vortex center. The mean, circumferentially-averaged circumferential velocity (V_θ) distributions of six (J,σ) conditions are shown in Fig. 4, along with the radial velocities (V_r) at $J = 0.76$ as a demonstration that V_r is negligible in all cases. It is evident that one may use an ideal vortex model to generally match the measured vortices. In other words, V_θ of the vortices shown here first increases almost linearly with radius like a forced vortex (viscous effect) and then decreases like a free vortex (potential effect). Burgers model (see Franc and Michel [10]), or Lamb-Oseen vortex (see Green [11]) can be used to fit the data (not shown):

$$V_\theta(r) = \frac{\Gamma}{2\pi r}\left(1 - e^{-1.256(r/a)^2}\right) \tag{4}$$

where Γ is the circulation of the vortex and a is the radial location where $V_\theta(r)$ is maximum. However, V_θ of the outer part of the vortex (the free-vortex part) decreases slower than a true free vortex, possibly due to the interaction with the propeller wake where excessive vorticity gets entrained to the outer part of the vortex.

Figure 4a compares V_θ profiles at $J = 0.90$, 0.78 and 0.76, and $\sigma = \sigma_{atm}$. Due to the high ambient pressure, no TVC occurs in either case (Table 1). It is clearly evident that the maximum V_θ ($V_\theta^{\max}$) and a of the vortex increases with decreasing J. Therefore, Γ of the vortex increases with decreasing J, conforming to the fact that the loading of the propeller increases with decreasing J. When $\sigma = \sigma_{2.5}$, as shown in Fig. 4b, not only the TVC status but also the trend of the V_θ profile changes. Between the cases of $J = 0.78$ and 0.76 at $\sigma = \sigma_{2.5}$, the trend of the V_θ profile with respect to $V_\theta^{\max}$ reverses as opposed to the cases at $\sigma = \sigma_{atm}$ while a keeps increasing (much more) with decreasing J. This phenomenon implies the key role the other phase of the fluid (either TVC or FMBC) plays in altering the flow structure of the tip vortex.

In order to elucidate this point, we rearrange the presentation of data of Fig. 4 and show the comparisons of V_θ of the same J at different σ in Fig. 5. At $J = 0.78$, as shown in Fig. 5a, $V_\theta^{\max}$ of the cavitating tip vortex ($\sigma = \sigma_{2.5}$) is significantly less than that of the non-cavitating one ($\sigma = \sigma_{atm}$), which somehow is expected due to the fact that the sheet cavitation attached to the propeller blade may cause unloading of the blade tip (Chow et al. [1]). Nevertheless, the cavitating tip vortex is much larger than the non-cavitating one while the diameter of the TVC is only about 0.2 ~ 0.3 mm, i.e., the volume expansion caused by the generation of the TVC doesn't catch up with the size increase of the tip vortex. The reason why this is so may lie somewhere else. One may look at this problem in the perspective of vortex strength (kinetic energy) and calculate the circulation Γ according to:

$$\Gamma = V_\theta^{\max} \cdot 2\pi a = \int_0^a \omega(r) \cdot 2\pi r dr \tag{5}$$

where $\omega(r)$ is the mean, circumferentially-averaged vorticity. Notice that when calculating Γ for a cavitating vortex the area occupied by the cavitation should be taken out of consideration. The results are: $\Gamma(J = 0.78, \sigma = \sigma_{2.5}) = 56.8$ m^2/s and $\Gamma(J = 0.78, \sigma = \sigma_{atm}) = 38.2$ m^2/s, i.e.,

$$\Gamma(J = 0.78, \sigma = \sigma_{2.5}) > \Gamma(J = 0.78, \sigma = \sigma_{atm}) \tag{6}$$

This is an interesting result in that it seems to suggest that the cavitating tip vortex obtains extra energy from some source(s) other than the mechanical work done by the propeller. One likely source which provides extra energy to the tip vortex is the cavitation process, i.e., the vaporization of water that does work to the liquid water by vapor cavity expansion. To confirm this speculation, more theoretical analyses involving thermodynamics need to be done to prove or disprove this theory.

Figure 5b shows the comparison between $V_\theta(J = 0.76, \sigma = \sigma_{2.5})$ and $V_\theta(J = 0.76, \sigma = \sigma_{atm})$. Similar to the cases of $J = 0.78$ (Fig. 5a), at $J = 0.76$ $V_\theta^{\max}(\sigma = \sigma_{2.5})$ is significantly less than $V_\theta^{\max}(\sigma = \sigma_{atm})$ and $a(\sigma = \sigma_{2.5})$ is much greater than $a(\sigma = \sigma_{atm})$, resulting in $\Gamma(\sigma = \sigma_{2.5}) = 84.4$ m^2/s and $\Gamma(\sigma = \sigma_{atm}) = 46.3$ m^2/s, i.e.,

$$\Gamma(J = 0.76, \sigma = \sigma_{2.5}) > \Gamma(J = 0.76, \sigma = \sigma_{atm}) \tag{7}$$

This time no TVC (i.e., no vaporization of water) but FMBC (i.e., many micro bubbles) involves in "energizing" the tip vortex. This result appears to be connected with the phenomenon of bubble drag reduction (McCormick and Bhattacharyya [12]). The mechanism of bubble drag reduction is still inconclusive. However, a theory proposed by Lo, L'Vov, and Procaccia [13] that shows the oscillation of bubble is the key to the drag reduction may have some implications on the energy budget of the FMBC-filled tip vortex. Again, advanced theoretical analyses are required.

2. Turbulence Characteristics:

The Reynolds stress (r_{ij}) is defined as:

$$r_{ij}(r,\theta)=\overline{u_i'u_j'} \tag{8}$$

where the over-bar denotes the phase-averaging operator, u_i' denotes the *i*-direction velocity fluctuation about the mean value, and *i*, *j* are indices that 1 represents the x-direction and 2 represents the y-direction. According to Benedict and Gould [14], the uncertainty in r_{ij}, Δr_{ij}, can be estimated using

$$\Delta r_{ij}=1.96\cdot[(1+C_{ij}^2)\overline{u_i'^2}\,\overline{u_j'^2}/N]^{1/2} \tag{9}$$

where $C_{ij}=r_{ij}/\left(\overline{u_i'^2}\,\overline{u_j'^2}\right)^{1/2}$ and $N=1000$ is the ensemble size. Therefore,

$$\Delta r_{11}/r_{11}=\Delta r_{22}/r_{22}=1.96\cdot[(1+1^2)/1000]^{1/2}\approx 8.8\% \tag{10}$$

We also use Eq. (3) to obtain the circumferentially-averaged Reynolds stress $R_{ij}(r)$. And the circumferentially-averaged turbulent kinetic energy (*k*) is defined as:

$$k(r)=\frac{1}{2}(R_{11}+R_{22}) \tag{11}$$

Figure 6a shows the *k* profiles of $J=0.90$, 0.78 and 0.76 at $\sigma=\sigma_{atm}$. The *k* distributions peak at the vortex center (the small deviation shown in the curve of $J=0.76$ is possibly due to the resolution being not fine enough for this region). Interestingly, the *k* peak value ($k^{\max}$) of $J=0.76$ is lower than that of $J=0.78$, despite the fact that the (mean) circulation of $J=0.76$ is greater than that of $J=0.78$. When $\sigma=\sigma_{2.5}$ as shown in Fig. 6b, $k^{\max}$ of both $J=0.76$ and 0.78 become much lower than that of $J=0.90$, with $k^{\max}$ of $J=0.76$ being the lowest. This phenomenon suggests that the other phase of the fluid (either TVC or FMBC) influences not only the mean flow but also the turbulence.

We rearrange Fig. 6 into Fig.7 to highlight the substantial differences between the cases of single-phase and multi-phase. Figs. 7a-b show almost 2/3 (67%) drop of $k^{\max}$ from single-phase cases to multi-phase cases. These turbulent kinetic energies may have two ways to go: one is the regular cascading process (a larger eddy breaks into smaller eddies) that *k* is finally dissipated by viscosity; the other is the inverse cascading process (smaller eddies merge into a larger eddy) that *k* is finally injected back to the mean flow. The "energized" mean tip vortex flows discussed previously seem to imply that *k* takes the latter route to help augment the mean flow. Following this argument, the vapor phase in the form of either TVC or FMBC must serve as an effective agent to inversely transfer energy from turbulent motions to mean flows.

CONCLUSION

PIV measurements are performed on the propeller tip vortex flow undergoing the process from non-TVC to TVC to FMBC conditions ($\sigma=\sigma_{2.5}$), as well as all-time non-TVC conditions ($\sigma=\sigma_{atm}$). It is clearly evident from our results that the vapor phase of the fluid in the form of either TVC or FMBC "energizes" the flow of the liquid phase by directly doing work on the flow and/or serving as an agent to extract energy from the turbulence to the mean flow. Our future works includes performing more detailed measurements in order to obtain the kinetic energy spectra of the flow to identify the role the TVC or the FMBC plays in the flow processes.

ACKNOWLEDGMENTS

This project is sponsored by the National Science Council of Taiwan under the grant number NSC-96-2628-E-019-030-MY2. The authors would like to thank Prof. Y.-Z. Kehr for the model propeller of his design used in the experiments. Also thanks are due to the graduate students of the PIV Lab and the MCT Lab at NTOU for their assistance in setting up and performing the experiments.

REFERENCES

[1] Chow, Y.-C., Lee, Y.-H., Hsin, C.-Y., 2009, "On a Peculiar Phenomenon of Fog-like Micro-Bubble Cluster Formation and its Mechanism Apparently Associated with Propeller Tip Vortex Cavitation," submitted to *Experiments in Fluids*.

[2] English, J. W., 1979, "Cavitation-Induced Hull Surface Pressures: Measurements in a Water Tunnel," Proceedings of symposium on propeller induced ship vibration, Royal Institution of Naval Architects, London, pp 1-11.

[3] Lee, S. J., Paik, B. G., Yoon, J. H., Lee, C. M., 2004, "Three-Component Velocity Field Measurements of Propeller Wake Using a Stereoscopic PIV Technique," *Experiments in Fluids*, 36, pp. 575-585.07-138.

[4] Calcagno, G., Di Felice, F., Felli, M., Pereira, F., 2002, "Propeller Wake Analysis Behind a Ship by Stereo PIV," Proc. 24th Symp. on Naval Hydrodynamics, Fukuoka, Japan.

[5] Chesnakas, C. J., Jessup, S. D., 2003, "Tip-Vortex Induced Cavitation on a Ducted Propulsor," Proc. 4th ASME/JSME Joint Fluids Eng. Conf., Honolulu, U.S.A. FEDSM2003-45320

[6] Oweis, G. F., Ceccio, S. L., 2005, "Instantaneous and Time-Averaged Flow Fields of Multiple Vortices in the Tip Region of a Ducted Propulsor," *Experiments in Fluids*, Vol. 38, pp. 615-636.

[7] Kim, S. E., Rhee, S. H., 2004, "Toward High-Fidelity Prediction of Tip-Vortex Around Lifting Surfaces," Proc. 25th Symp. on Naval Hydrodynamics, St. John's, Canada.

[8] Rhee, S. H., Joshi, S., 2005, "Computational Validation for Flow around a Marine Propeller Using Unstructured Mesh Based Navier-Stokes Solver," *JSME International Journal*, Series B, Vol. 48, No. 3, pp. 562-570.

[9] Chen, B., 2000, "RANS Simulation of Tip Vortex Flow for a Finite-Span Hydrofoil and a Marine Propulsor," Ph.D. thesis, The University of Iowa, Iowa City, IA.

[10] Franc, J.-P., Michel, J.-M., 2004, *Fundamentals of Cavitation*, Kluwer Academic Publishers, Dordrecht, The Netherlands.
[11] Green, S. L. 1995, *Fluid Vortices,* Kluwer Academic Publishers, Dordrecht, The Netherlands.
[12] McCormick, M. E., Bhattacharyya, R., 1973, "Drag Reduction of a Submersible Hull by Electrolysis," *Naval Engineers Journal*, Vol. 85, No. 2, pp. 11-16.
[13] Lo, T. S., L'Vov, V. S., Procaccia, I., 2006, "Drag Reduction by Compressible Bubbles," *Physical Review E*, Vol. 73, No. 3, p 036308.
[14] Benedict, L. H., Gould, R. D., 1996, "Towards Better Uncertainty Estimates for Turbulence Statistics, " *Experiments in Fluids*, Vol. 22, No. 2, pp. 129 – 136.

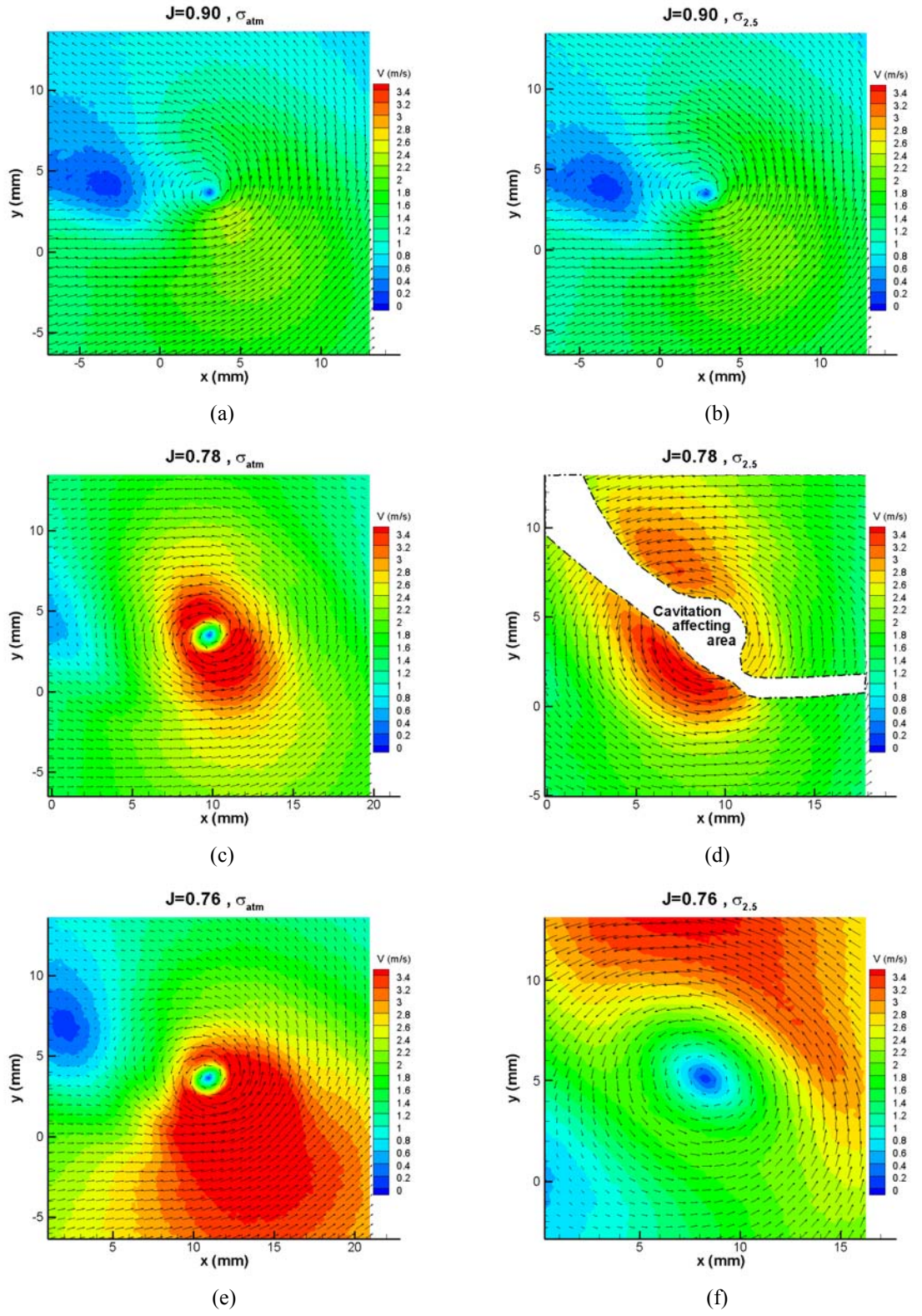

Figure 3: Mean-flow induced velocity vector maps at conditions of (a) $J = 0.90$ and $\sigma = \sigma_{atm}$, (b) $J = 0.90$ and $\sigma = \sigma_{2.5}$, (c) $J = 0.78$ and $\sigma = \sigma_{atm}$, (d) $J = 0.78$ and $\sigma = \sigma_{2.5}$, (e) $J = 0.76$ and $\sigma = \sigma_{atm}$, and (f) $J = 0.76$ and $\sigma = \sigma_{2.5}$. Contour plots indicates the velocity magnitudes.

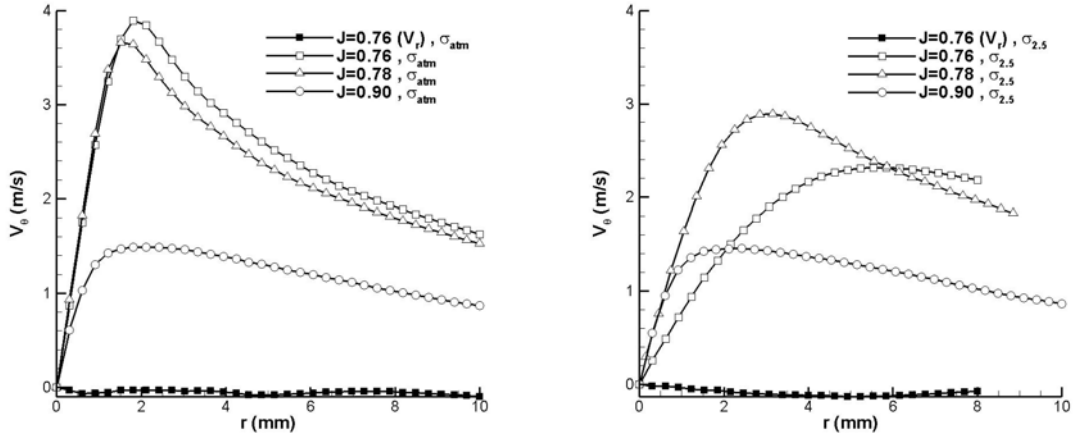

(a) (b)

Figure 4: Circumferential velocity distributions $V_\theta(r)$ of varying J at conditions of (a) $\sigma = \sigma_{atm}$, and (b) $\sigma = \sigma_{2.5}$.

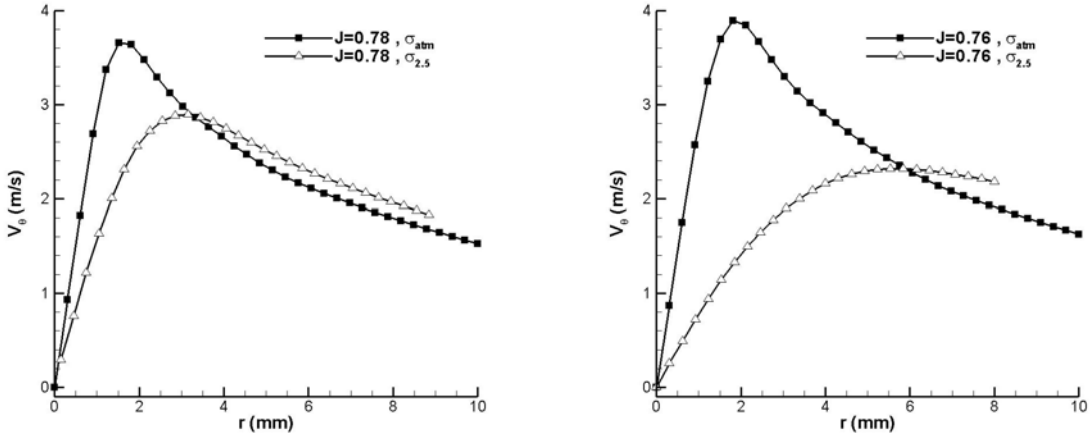

(a) (b)

Figure 5: Circumferential velocity distributions $V_\theta(r)$ of varying σ at conditions of (a) $J = 0.78$, and (b) $J = 0.76$.

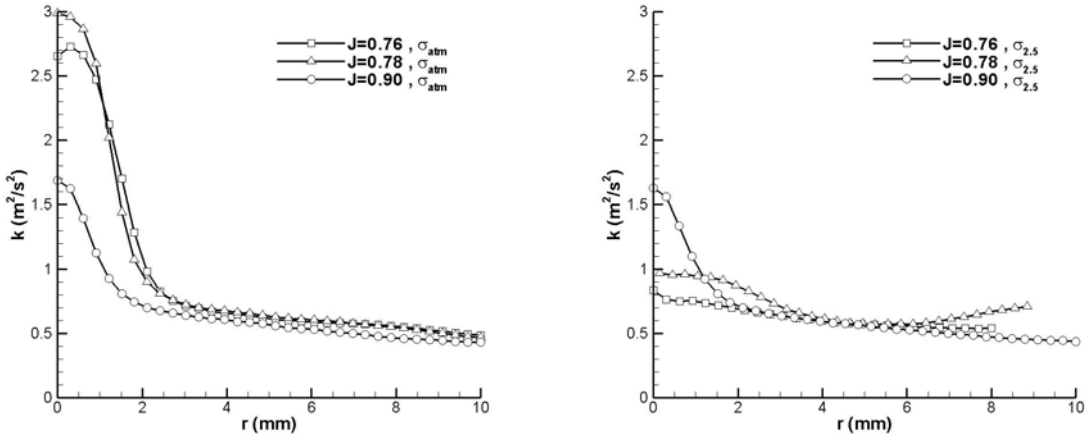

(a) (b)

Figure 6: Turbulent kinetic energy distributions $k(r)$ of varying J at conditions of (a) $\sigma = \sigma_{atm}$, and (b) $\sigma = \sigma_{2.5}$.

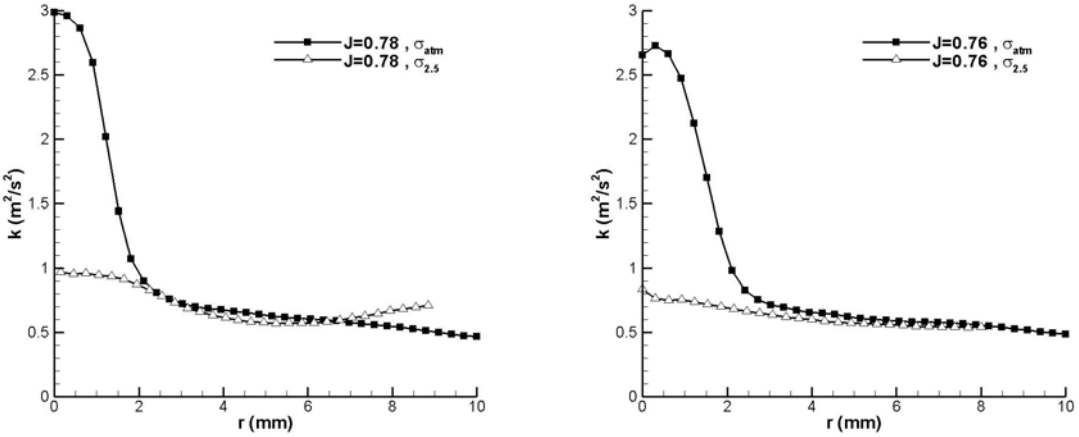

(a) (b)

Figure 7: Turbulent kinetic energy distributions $k(r)$ of varying σ at conditions of (a) $J = 0.78$, and (b) $J = 0.76$.